SHOCK-INDUCED CO_2 LOSS FROM $CaCO_3$: IMPLICATIONS FOR EARLY PLANETARY ATMOSPHERES

by
Manfred A. Lange[1)]
and
Thomas J. Ahrens

Seismological Laboratory 252-21, California Institute of Technology
Pasadena, CA 91125

1) Now at Alfred-Wegener-Institute for Polar Research, Columbus Center, D-2850 Bremerhaven, Fed. Rep. of Germany

December 18, 1984

ABSTRACT

We report new results of shock recovery experiments on single crystal calcite. Recovered samples are subjected to thermogravimetric analysis. This yields the amount of post-shock CO_2, the decarbonization interval, ΔT, and the activation energy, ΔAE, for the removal of remaining CO_2 in shock-loaded calcite. Comparison of post-shock CO_2 with that initially present determines shock-induced CO_2 loss as a function of shock pressure. Incipient to complete CO_2 loss occurs over a pressure range of ~10 to ~70 GPa. Comparable to results on hydrous minerals, ΔT and ΔAE decrease systematically with increasing shock pressure. This indicates that shock loading leads to both the removal of structural volatiles and weakening of bonds between the volatile species and remainder of the crystal lattice.

Optical and scanning electron microscopy (SEM) reveal structural changes, which are related to the shock-loading. Comparable to previous findings on shocked antigorite is the occurrence of dark, diffuse areas, which can be resolved as highly vesicular areas as observed with a scanning electron microscope. These areas are interpreted as representing quenched partial melts, into which shock-released CO_2 has been injected.

The experimental results are used to constrain models of shock-produced, primary CO_2-atmospheres on the accreting terrestrial planets.

Introduction

Carbonate rocks are present in nearly all terrestrial shallow marine sedimentary basins. Carbonates, thus, comprise the most abundant non-hydrous volatile contained in rocks, amounting to about 20% by volume of the Earth's sedimentary rocks and storing a substantial part, if not most, of the terrestrial CO_2 inventory. Although only a minor constituent of the terrestrial atmosphere, CO_2, next to water, is the second most abundant volatile specie on Earth. [1]

About 30% of all terrestrial impact structures have been formed in carbonate-bearing rocks [2]. Kieffer and Simonds [2] postulate that the effect of rapidly expanding CO_2, released from the carbonates during impact, leads to the complete dispersion and subsequent erosion of impact melt, resulting in the observed deficiency of impact melt layers in impact structures formed in carbonate rocks. Since carbonates apparently buffer the CO_2 pressure of the Venus atmosphere [4], it is likely that a significant fraction of the impacts on both Venus and the Earth involve carbonate rocks. In the case of Mars, CO_2, pressure is now buffered by quasi-permanent solid CO_2 ice cap at the martian south pole, whether carbonates now or previously, stored a significant CO_2 inventory on that planet is less clear [3].

At present, a major source of the earth's atmospheric CO_2 results from both decay of organic matter of volcanic activity associated with subduction. Recycling of CO_2 and H_2O from calcareous and hydrous oceanic sediments are believed to take place at subduction zones. It is possible that prebiotic carbonates were present on the earth and on Mars and Venus. Thus impact-induced release of CO_2 from carbonates could have played a role in the formation and evolution of the atmosphere.

Recently, we proposed a model for the formation of an impact-generated atmosphere/hydrosphere on Earth, which results from the release of H_2O due to shock heating of hydrous phyllosilicates in the accretional environment of the Earth [5, 6, 7]. We could invoke similar models for the generation of a primary CO_2 atmosphere. However, while it is thought that structural water, contained in hydrous minerals within accreting planetesimals, provides a direct source for atmospheric water [8, 9], calcite [$CaCO_3$], although ubiquitous in class I and II

carbonaceous chondrites [10, 11] cannot be proposed in the same sense as the primary atmospheric CO_2 source because of its small abundance in accreting planetesimals. Instead, the following chain of reactions could lead to the build-up of a primary CO_2 atmosphere on the terrestrial planets:

$$Mg_3Si_2O_5(OH)_4 \xrightarrow[impact]{} 2\,H_2O + Mg_2SiO_4 + MgSiO_3 \quad (1)$$

$$2\,H_2O \rightarrow 2H_2 + O_2 \quad (2)$$

$$CH_4\,(X) + 2O_2 \xrightarrow[impact]{} CO_2 + H_2O \quad (3)$$

$$C(X) + O_2 \xrightarrow[impact]{} CO_2 \quad (4)$$
(graphite)

$$CaSiO_3\,(X) + CO_2 \rightarrow CaCO_3 + SiO_2 \quad (5)$$

where (X) indicates the phase brought to the planet within the infalling planetesimals. The planetesimals, which produced the terrestrial planets, are assumed to contain both hydrous phyllosilicates (Eq. 1), as well as hydrocarbons (represented by CH_4 in equation (3)). While organic matter may comprise up to 30% of the total carbon in carbonaceous chondrite-like planetesimals [12], it is known that most of the elemental carbon is present as graphite or in a graphite-like phase [13]. Both carbon sources react with previously derived oxygen (equation (2)) to form CO_2. Under appropriate temperature conditions, the Urey-type reaction (equation (5)) will then yield carbonates on the crust of the accreting planet. Impact on carbonates would subsequently give rise to CO_2 atmospheres on Mars and Venus and probably produced a CO_2-rich primordial atmosphere on Earth [14] via the following reaction:

$$CaCO_3 \xrightarrow[impact]{} CaO + CaO_2 \quad (6)$$

The parameter needed to describe these processes as well as for cratering phenomena in carbonate rocks is the threshhold pressures which lead to incipient to complete CO_2 loss from carbonates. Determination of these pressures is the major objective of this paper. We have performed shock-recovery experiments aimed to determine the amount of shock-induced CO_2 loss in calcite

($CaCO_3$) as a function of shock pressure. Optical and scanning electron microscopy was used to document structural changes in the shock-loaded samples and to reveal some of the processes related to shock-induced decarbonization.

Experimental Details

Calcite samples (variety Iceland Spar from Chihuahua, Mexico; initial density 2.719 ± 0.002 g/ cm^3) were cut into cylindrical samples ~ 4 mm in diameter and were ground flat and parallel to a mirror finish and a thickness of ~ 0.5 mm. The samples were then inserted in specially designed stainless steel target containers, which provide an escape path for gaseous decomposition products (i.e., CO_2; cf. [6]). The target containers were placed in a fixture attached to the Caltech 20 mm propellent gun and were impacted by lexan projectiles bearing disk-shaped 2024 aluminum and 304 stainless steel flyer plates. Impacts of the projectiles at velocities of 1.2 to 1.8 km/s resulted in peak shock pressures (i.e., reverberated pressures) in the samples of 15 to 42 GPa (Table 1). Initial and peak shock pressures were calculated via the impedance match method [24] using the shock wave standards of McQueen et al.

Immediately after each shot, the sample material was carefully recovered and parts of it were used for thermogravimetric analysis employing a Mettler Model 2000C Thermoanalyser. This analysis provided the amount of post-shock CO_2 in each sample and comparison with the initially present CO_2 (as determined on a reference sample; Table 1) yielded the mass of shock-induced CO_2 lost from the sample. The present experiments were carried out in assemblies which vented into air, hence release occurs to partial pressure of CO_2 of ~ 10^{-3} bar. Tyburczy and Ahrens [23] point out that the shock pressure range required to devolatilize carbonates depends on the partial pressure of CO_2 in the container. Greater shock pressures are expected to be required if impact takes place in a tank which captures the CO_2-rich propellant gas. They point out that the difference in the partial pressure of CO_2 between the present experiments and those of Kotra et al. [26] may explain the lack of observing CO_2 losses in shocked calcite in those experiments.

Results

a) Thermogravimetry

Results of the thermogravimetric analysis (Table 1 and Figures 1-3) demonstrate a single relationship between shock-induced CO_2 loss and peak shock pressure. Since most of the entropy production, leading to the release of CO_2 from shocked calcite upon pressure unloading takes place as a result of the initial shock, shock-induced CO_2 loss is also given as a function of initial shock pressure (i.e., prior to reverberation of the shock wave in the higher impedance stainless steel sample container). Thus, peak pressures required to result in a certain loss of CO_2 probably represent maximum pressure estimates. For some natural impact situations shock reverberation is absent, therefore, the direct shock pressure more closely describes the peak shock produced for an impact at a given velocity.

The sample mass, versus, temperature data used to derive post-shock CO_2 content, are useful in another context. As can be seen in Table 1, decarbonization temperatures (i.e., the median of the temperature interval over which loss of CO_2 is observed) vary unsystematically between ~ 930 to 990 K and are insensitive to shock pressure. The range of decarbonization temperatures (found in our experiments) agrees well with values found for decomposition of unshocked calcite by other investigators at ambient CO_2 partial pressures (i.e., 991 K; [15]).

The decarbonization interval (i.e., the temperature interval over which decomposition and loss of CO_2 occurs) varies systematically with the shock pressure to which the sample was exposed. We note this interval decreases with increasing shock pressure (Table 1, Figure 2). The same can be said to the closely related activation energy needed to remove the (post-shock) CO_2 (Figure 3, cf. [6]). For both quantities, a linear relation between their (logarithmic) values and the shock pressure can be obtained:

$$\Delta T(K) = 184.5 - 2.4\ P\ (GPa) \tag{7}$$

$$\log_{10} \Delta AE\ (kcal/\ mole) = 1.01 - 0.01\ P(GPa) \tag{8}$$

where ΔT and ΔAE are decarbonization interval and activation energy, respectively, and P is the peak shock pressure.

b) Optical and Scanning Electron Microscopy

The unshocked sample material is comprised of clear, colorless, single crystals with no observable cracks. Upon shock-loading, the following major textural changes can be observed under an optical microscope in reflected light (Figure 4):

(i) dark, narrow cleavage cracks running, in most cases, across the entire sample disc; as expected, such cracks are often parallel or subparallel to cleavage

(ii) broader, diffuse elongated, dark areas, which often run perpendicular to the type (i) cracks; the latter cracks are often set off to each other on either side of the broader crack

(iii) more or less randomly distributed, patchy dark areas, resembling in some respects the type (ii) features

(iv) large, single, dark to vesiculated appearing areas. The vesicles are in the sub-millimeter range; under crossed nicols, these areas (as well as the type (iii) features) display a characteristic bright glow of diffuse light comparable to observations of similar features in shocked serpentine [17] and shocked mica [18].

It should be noted that the occurrence of all four of the above features are present only in only the most heavily shocked samples, whereas low and moderately shocked samples display mostly type (i) to (iii) features. However, there is no systematic transition from type (i) to type (iv) features with e.g., increasing pressure.

Figures 5 and 6 show a polished thin section of sample 7, the highest shocked sample. It can be seen that there is a fairly large, vesiculated area (type (iv)) close to the sample edge. At higher magnification (Figure 6), it is observed that dark and light particles are contained in the clear, unchanged sample material in close contact to each other.

Under the scanning electron microscope (SEM), details of this region of sample 7 are observed. It appears that the dark features seen in the optical microscope are comprised of irregularly shaped vesicles and open cracks. This observation parallels shocked antigorite serpentine, where dark veins were

resolved as vesicular areas under the SEM [17]. At higher magnification (Figure 7b), it is seen that open cracks are, at some places, filled by small (<1 to 5 μm) particles. This suggests that the openings were produced by a, now absent, fluid which deposited the small particles. Figure 8 is taken of another area of sample 7, nearer the center of the sample disc and situated in one of the dark spots seen with the optical microscope (feature (iii)). These SEM pictures reveal the sponge-like character of the vesicular areas. It is seen that vesicles are irregularly formed and that two or more vesicles often form a larger void. The light, highly reflecting spots represent metal (stainless) steel particles from the sample holder. The latter chemistry was inferred by spot energy dispersive X-ray analysis.

Discussion

An important result of this study is the relation between shock-induced CO_2-loss and shock pressure in calcite samples. This parallels findings of comparable studies on brucite ($Mg(OH)_2$) and serpentine ($Mg_3Si_2O_5(OH)_4$), which show a systematic relationship between shock-induced water loss and shock pressure [6, 7]. Figure 9 compares the present results with the data on the hydrous minerals and gives the ranges in pressure for incipient to complete volatile loss (the latter as theoretical estimates of [2] and [19]) for each mineral.

Two major points should be noted: (i) the scatter in the volatile loss versus shock pressure curves is largest for the calcite samples, and (ii) the pressure range for incipient to complete volatile loss, ΔP, is also largest for calcite (~60 GPa compared with ~25 and 40 GPa for brucite and serpentine, respectively).

A possible explanation for these observations could be the occurrence of localized, inhomogeneous heating, which would lead to zones of elevated temperatures (and thus loss of CO_2 from these zones) at low and moderate shock pressures. Recently, Kondo and Ahrens [20] have reported data, which strongly support the model of shear band heating [21], which results in localized temperatures, well in excess of computed continuum temperatures. Thus, even at lower shock pressures, parts of the sample will be strongly heated and will lose its structural CO_2, while at higher pressures more homogeneous heating of the

sample takes place. This, together with high decarbonization temperatures (990 K as compared with 610 and 850 K for dehydration of brucite and serpentine, respectively) explains the higher shock pressures required for complete loss of CO_2 in calcite. It should also be noted that calcite contains the greatest relative quantity of a volatile among the three minerals under consideration, i.e., 43 wt.% versus 31 and 13 wt. % for brucite and serpentine, respectively. Thus, relatively more energy has to be expended in breaking the bonds between the volatile and non-volatile components of the respective crystal lattices. This might be another explanation for the larger range in pressure for incipient to complete loss of CO_2 in calcite.

The shear-band-heating model is supported by the microscopic observations. As noted above, indications for mechanical deformation (shear bands) are abundant in all of the samples, covering a range in pressure of 15 to 42 GPa. In contrast, shocked antigorite serpentine shows remarkably little indication of shock-induced deformation [17], which suggest that shear band (inhomogeneous) heating may be less important in this mineral.

Type (i) and (ii) deformational features (figure 4) appear to be related to the major cleavage planes in calcite $\{10\bar{1}1\}$. While cleavage in calcite is perfect, it is known that serpentine does not display any prominent cleavage planes [16], in agreement with our observations of shocked material.

A consequence of the intense, localized heating in shocked calcite is the production of partial melt, presumably while still under high pressure [25]. At the lower shock pressures it is confined to narrow, elongated zones along major cleavage planes (type (i) and (ii) features). However, as noted above, larger areas of high temperatures can also be inferred for low to moderately shocked samples as indicated by the occurrence of type (iii) features. Only the large, diffuse and vesiculated areas (type (iv)) require greater shock pressures. Parallel to the occurrence of incongruent melting is the loss of structural CO_2 in shocked calcite. CO_2 loss takes place upon decompression of the shock loaded sample, allowing the evolving gas to expand and to leave the sample and the sample container. We suggest that some of this gas gets trapped in the partially molten zones, where it leads to the observed vesicular textures. The irregularly

formed and partly tear drop-shaped vesicles, as seen in the SEM (see figures 7 and 8) are evidence for the dynamic character of this process. This applies also to the apparently moved fragments, which fill cracks and voids in the samples (figure 7b). We interpret this observation as representing small particles being driven into these cracks by the expanding CO_2 gas.

The observation of decreasing decarbonization interval, ΔT, and decreasing activation energy for removal of post shock CO_2, ΔAE, with increasing shock pressure is also seen in shock loaded antigorite [5, 17]. It should be noted that the scatter of the values of ΔT and ΔAE versus shock pressure (figures 2 and 3) is less than the scatter in the measured shock-induced CO_2 loss versus shock pressure data (figure 1). Shear band heating leads to a decarbonization behavior, which cannot as clearly be related to shock pressure (thus the larger scatter) as in the more homogeneously heated serpentine, where H_2O loss is more unequivocally related to shock pressure. On the other hand, shock loading of calcite leads, independent of localized thermal effects, to a weakening of bonds between CO_3 groups and CaO. Thus, increasing shock pressure leads to systematic enhancement of CO_3 mobility in subsequent heating, independent of local thermal effects. This will result in smaller ΔT and ΔAE values in shocked calcite as compared to unshocked samples, as seen in our data.

The decrease in ΔT and ΔAE with increasing shock pressure has an additional implication. If we assume that a second shock leads to a further decrease in the bonding strength between CO_3 and CaO, we infer that multiple shocks will lead to CO_2 losses, which would require much higher shock pressures in a single shock event. Thus we conjecture that multiple shocks result in enhanced CO_2 release in shock loaded calcite.

Conclusions/Implications

Volatile-bearing minerals (brucite, serpentine, calcite) lose their structural gases as a result of shock loading. Shock-induced volatile loss increases systematically with shock pressures. In addition, shock loading leads to increasingly weakened bonds between the volatile and non-volatile components of these minerals as indicated by decreasing devolatilization intervals and decreasing

activation energy for removal of post-shock volatiles with increasing shock pressure. Optical and scanning electron microscopy demonstrate textural changes which appear to be related to the release and the rapid escape of volatiles. Production of melt and devolatilization results in vesicular zones. In the case of calcite, localized devolatilization via shear band heating causes the release of CO_2 at relatively low shock pressures. The relation between CO_2 loss and shock pressure is less consistent for calcite as compared to data for water loss versus pressure in hydrous minerals.

CO_2 is not likely to be a copious constituent of accreting planetesimals in the early solar system. Instead, it is assumed that calcite or other carbonate minerals are formed indirectly by a chain of reactions (eqs. (1) - (5)) involving silicates, water and hydrocarbons and/or graphite in accreting planetesimals. Shock loading of the resulting carbonates as a result of impact of infalling planetesimals on the surface of a growing planet would then lead to release of CO_2 via reaction (6) and could give rise to a primary, CO_2-rich atmosphere on Venus, Mars, and Earth.

Using equation of state data for calcite [22], shock pressures, required for a certain CO_2 loss can be related to impact velocities. If we assume that impact velocities of infalling planetesimals equals the escape velocity of the growing terrestrial planet, we can specify stages in the accretional sequences which correspond to a certain degree of CO_2 production from impact upon surface material. Figure 10 shows the shock-induced CO_2-generation as a function of the relative radius r/R (R = final planetary radius) and relative mass m/M (M = final planetary radius) and relative mass m/M (M = final planetary mass of planet) for Earth, Venus, and Mars. As can be seen, complete loss of CO_2 from calcite and thus, the potential growth of a CO_2-rich atmosphere occurs on Earth and Venus after both have grown to about 60% of their final size. Mars never reaches this stage during its accretion due to its smaller size and lower mean density.

Finally we note the effect of partial pressure of CO_2 on the yield shock induced CO_2 production that has recently been pointed out by Tyburczy and Ahrens [23]. The parallel effect of the partial pressure of H_2O on the impact dehydration of water-bearing minerals [5, 6] needs to be quantified in future

work.

Acknowledgments:

We appreciate the assistance of W. Ginn, E. Gelle, and M. Long in the experiments and the use of the thermogravimetric analyzer and advice proffered by G. Rossman and R. Haines. Comments on this research offered by J. Tyburczy were very helpful. M. Lange was supported by a stipend of the Deutsche Forschungsgemeinschaft during his stay at Caltech. This work is supported under NASA grant NGL-05-002-105, Division of Geological and Planetary Sciences, California Institute of Technology, Pasadena, CA 91125, Contribution number 4166.

References

1 A. B. Ronov and A. A. Yaroshefskiy, Chemical structure of the Earth's crust, Geochim. Int. 4 (1967) 1041-1066.

2 S. W. Kieffer and C. H. Simonds, The role of volatiles and lithology in the impact cratering process, Rev. Geophys. Space Sci. 18 (1980) 143-181.

3 M. C. Booth and A. A. Kieffer, Carbonate formation in mars-like environment, J. Geophys. Res. 83 (1978) 1809-1815.

4 J. S. Lewis and F. A. Kreimendahl, Oxidation state of the atmosphere and crust of Venus from Pioneer-Venus results, Icarus 42 (1980) 330-337.

5 M. A. Lange and T. J. Ahrens, The evolution of an impact-generated atmosphere, Icarus 51 (1982a) 96-120.

6 M. A. Lange and T. J. Ahrens, Impact-induced dehydration of serpentine and the evolution of planetary atmospheres, Proc. Lunar Planet. Sci. Conf. 13th, J. Geophys. Res. 87, Suppl. (1982) A451-A456.

7 M. A. Lange and T. J. Ahrens, FeO and H_2O and the homogeneous accretion of the earth, submitted to Earth Planet. Sci. Lett. (1983).

8 G. Arrhenius, B. R. De, and H. Alfvén, Origin of the ocean, in The Sea, Vol. 5, E. D. Goldberg (ed.) (Wiley, N. Y., 1974) 839-861.

9 A. E. Ringwood, Origin of the Earth and Moon (Springer Verlag, New York/Berlin, 1979).

10 B. Nagy, Carbonaceous Meteorites (Elsevier, Amsterdam/N. Y., 1975).

11 B. Mason, The mineralogy of meteorites, Meteoritics 7 (1972) 309-326.

12 R. H. Becker and S. Epstein, Carbon, hydrogen, and nitrogen isotopes in solvent-extractable organic matter from carbonaceous chondrites, Geochim. Cosmochim. Acta, 46 (1982) 97-103.

13 S. Chang and R. Mack, Carbon chemistry of separated phases of Murchison and Allende meteorites (abstract), in Lunar and Planetary Science IX

(Lunar and Planetary Institute, Houston, TX, 18) 157-159.

14 M. H. Hart, The evolution of the atmosphere of the earth, Icarus, 33 (1978) 23-39.

15 P. G. Nutting, Some standard thermal dehydration curves of minerals, U.S. Geol. Surv. Prof. Pap., 197-E (1943) 197-216.

16 W. A. Deer, R. H. Howie, and J. Zussman, Rock-Forming Minerals (Wiley, N. Y., 1964).

17 M. A. Lange, P. Lambert, and T. J. Ahrens, Shock effects on hydrous minerals and implications for carbonaceous meteorites, submitted to Geohim. Cosmochim. Acta (1983).

18 P. Lambert and I. D. R. Mackinnon, Micas in experimentally shocked gneiss, submitted to Proc. Lunar Planet. Sci. Conf. 14th (1983).

19 M. A. and T. J. Ahrens, The evolution of an impact-generated atmosphere (abstract), in Lunar and Planetary Science XI (Lunar and Planetary Institute, Houston, TX, 1980) 596-598.

20 K. Kondo and T. J. Ahrens, Heterogeneous shock-induced thermal radiation in minerals, Phys. Chem. Minerals, 9 (1983) 173-181.

21 D. E. Grady, Processes occurring in shock compression or rocks and minerals, in High Pressure Research: Applications to Geophysics, M. H. Manghnani and S. Akimoto (eds.) (Academic Press, N. Y., 1977), 389-438.

22 G. A. Adadurov, B. D. Balashov, and A. N. Dremin, A study of the volumetric compressibility of marble at high pressures, Bull. Acad. Sci. U. S. S. R., Geophys. Ser., no. 5 (1961) 463-466.

23 J. A. Tyburczy and T. J. Ahrens, Dynamic compression and volatile release of carbonates, submitted to J. Geophys. Res. (1984).

24 R. G. McQueen, S. P. Marsh, J. W. Taylor, J. N. Fritz, and W. J. Carter, The equation of state of solids from shock wave studies, in High-Velocity

Impact Phenomena, edited by R. Kinslow, 293-417, Academic Press, New York (1970).

25 W. L. Huang and P. J. Wyllie, Melting relationships in the systems $CaO-CO_2$ and $MgO-CO_2$ to 33 kilobars, Geochim. Cosmochim. Acta 40, 129-132 (1976).

26 Kotra, R. K., J. H. See, E. K. Gibson, F. Hörz, M. J. Cintala, and R. S. Schmidt, Carbon dioxide loss in experimentally shocked calcite and limestone, Abstract, Lunar and Planetary Science 14, 401-402.

Table 1: Experimental data for shock recovery experiments on calcite

Sample No.	weight, mg	Impactor velocity, km/s	material[1]	Initial Peak pressure, GPa		CO_2 loss[2], wt. %	Decarbonization temperature K	Decarbonization interval K	Activation energy, kcal/mole
unshocked						42.7[3]	995	200	10.4
CA-1	26.3	1.22	Al	9.5	15.4	30.0	942	130	8.5
CA-2	25.2	1.53	Al	12.5	20.4	55.5	945	125	5.4
CA-3	25.4	1.32	SS	14.5	26.6	54.6	951	125	5.6
CA-4	25.3	1.50	SS	17.0	34.0	62.0	967	100	3.6
CA-5	25.4	1.54	SS	17.5	34.6	59.8	993	99	4.3
CA-6	25.8	1.72	SS	20.5	41.0	57.1	973	99	4.5
CA-7	25.2	1.80	SS	21.0	42.0	67.4	978	80	3.6
CA-8[4]	19.6	1.61	Al	14.3		10.6	927	177	not determined

1) Al = 2024 aluminum; SS = 304 stainless steel

2) CO_2 loss compared to initial CO_2 content of calcite samples

3) CO_2 content of pristine sample material in wt. % of the sample mass

4) control experiment employing aluminum target container resulting in less shock reverberations

Figure Captions

Figure 1: Shock-induced CO_2 loss versus peak and initial shock pressure in single crystal.

Figure 2: Temperature interval ΔT for loss of CO_2 in thermogravimetric analysis of shock calcite versus peak shock pressure.

Figure 3: Activation energy for the loss of CO_2 in thermogravimetric analysis of shock loaded calcite versus peak shock pressure.

Figure 4: Reflected light photomicrograph of shocked calcite (41 GPa) (i) - (iv) indicate deformational features (see text).

Figure 5: Reflected light photomicrograph of shocked calcite (42 GPa). Note the vesicular area at the upper left edge of the sample.

Figure 6: Detail of photomicrograph of figure 5, showing the upper left edge of the sample disc. Scale bar in this and the following figures in microns.

Figure 7: a) Detail of area enclosed in dashed box in figure 6, as seen under the scanning electron microscope (SEM). b) SEM picture of area A in Figure 7a) at higher magnification.

Figure 8: a) and b) SEM pictures of highly vesicular areas of shocked calcite sample (42 GPa). Depicted are dark areas in the center part of figure 5.

Figure 9: Shock-induced volatile loss as a function of shock pressures for calcite, brucite and antigorite. Data on the hydrous minerals are from [6] and [7]; theoretical estimates for complete devolatilization are given by [2] and [19].

Figure 10: Shock-induced CO_2 loss in calcite (in wt.% of the total CO_2 content) versus relative size (r/R) and relative mass (m/M) for Earth ($\oplus$), Venus (φ), and Mars (σ).

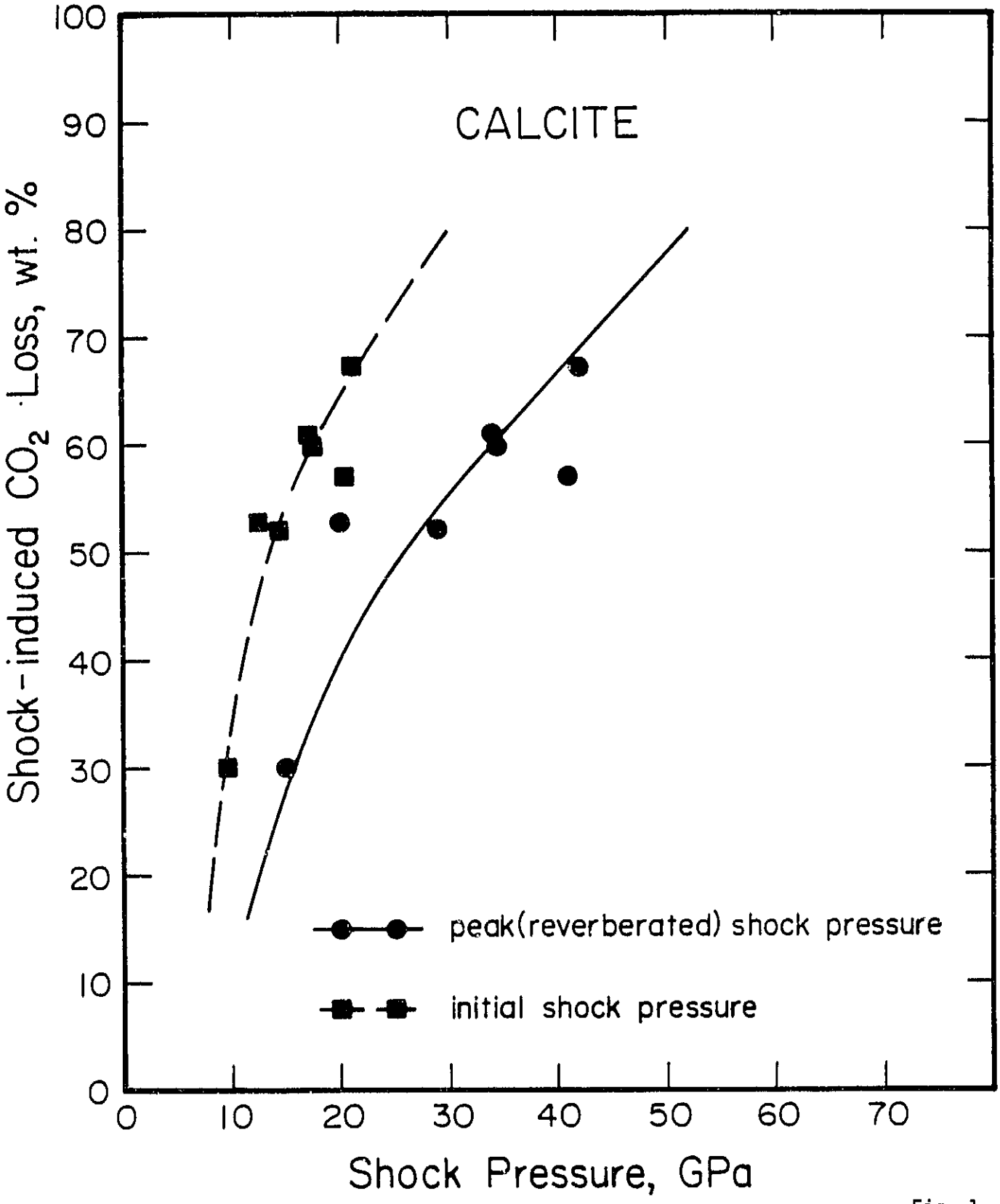

Fig. 1

TJA84196SFD

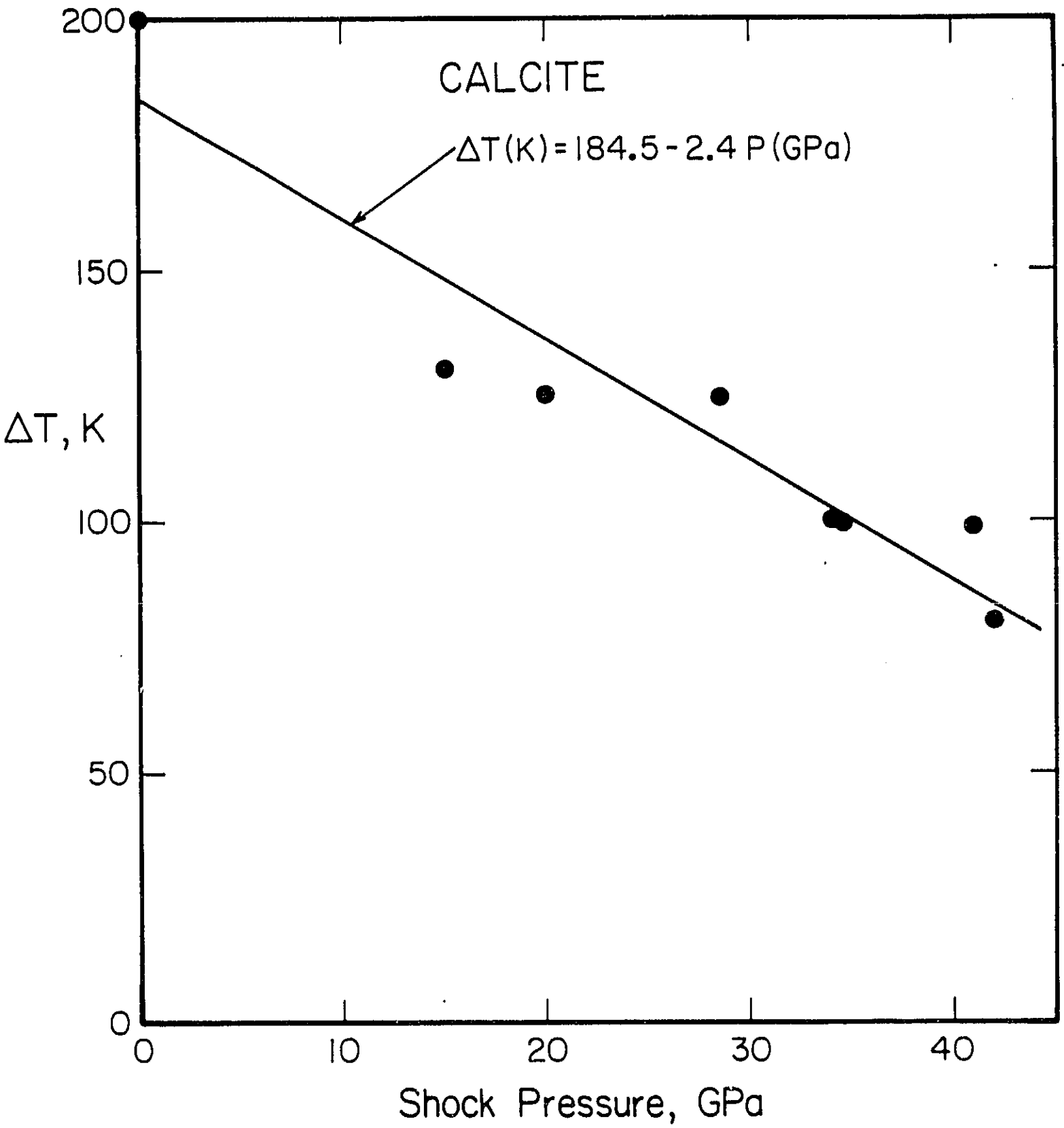

Fig. 2

TJA84197SFD

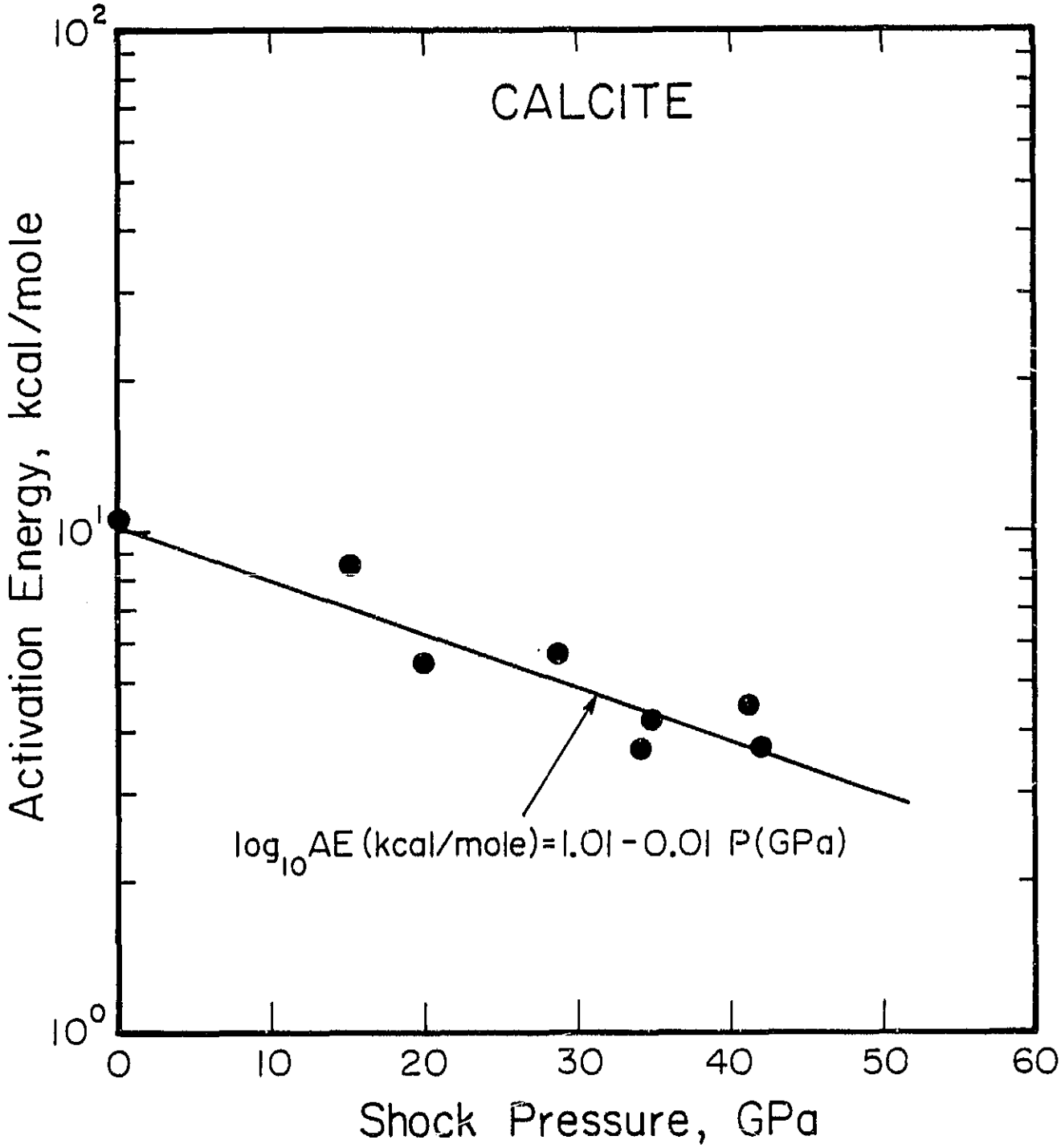

Fig. 3

TJA84198SFD

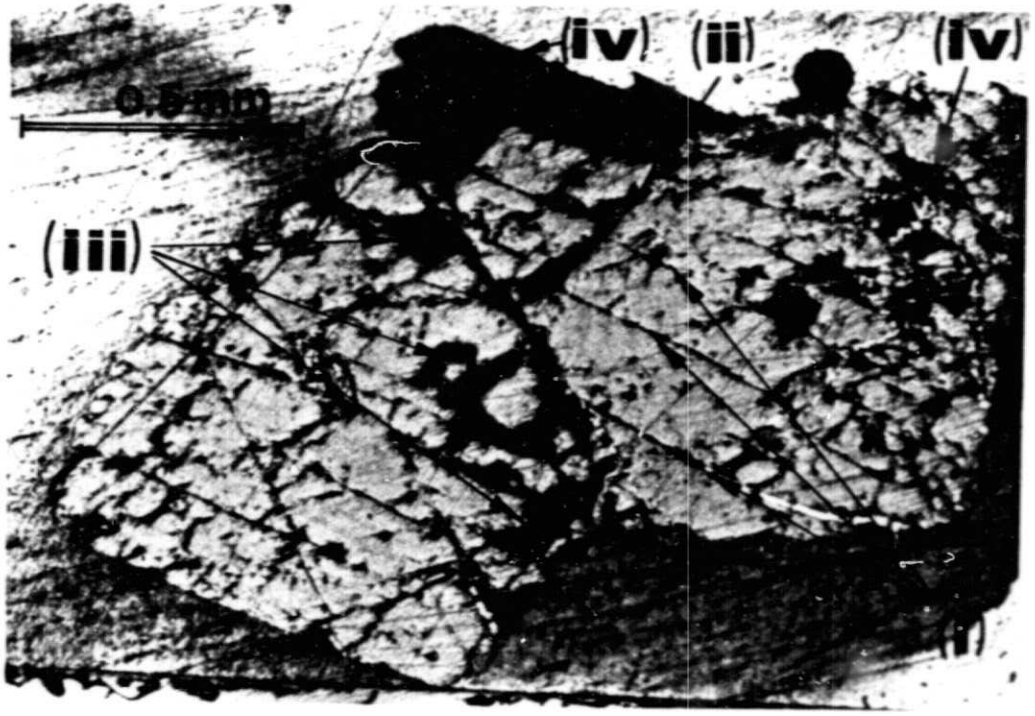

Fig. 4

TJA84199SFD

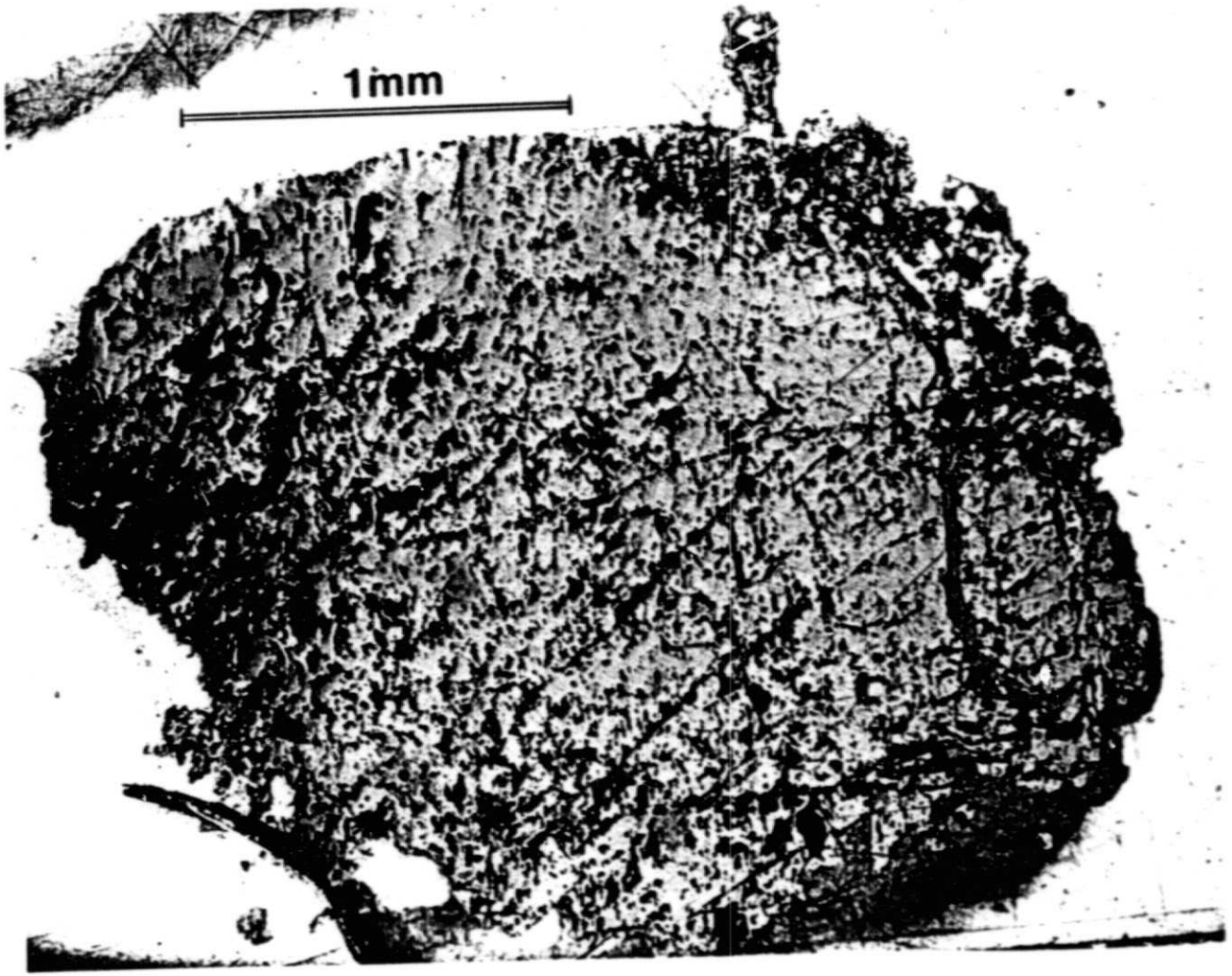

Fig. 5

TJA84200SFD

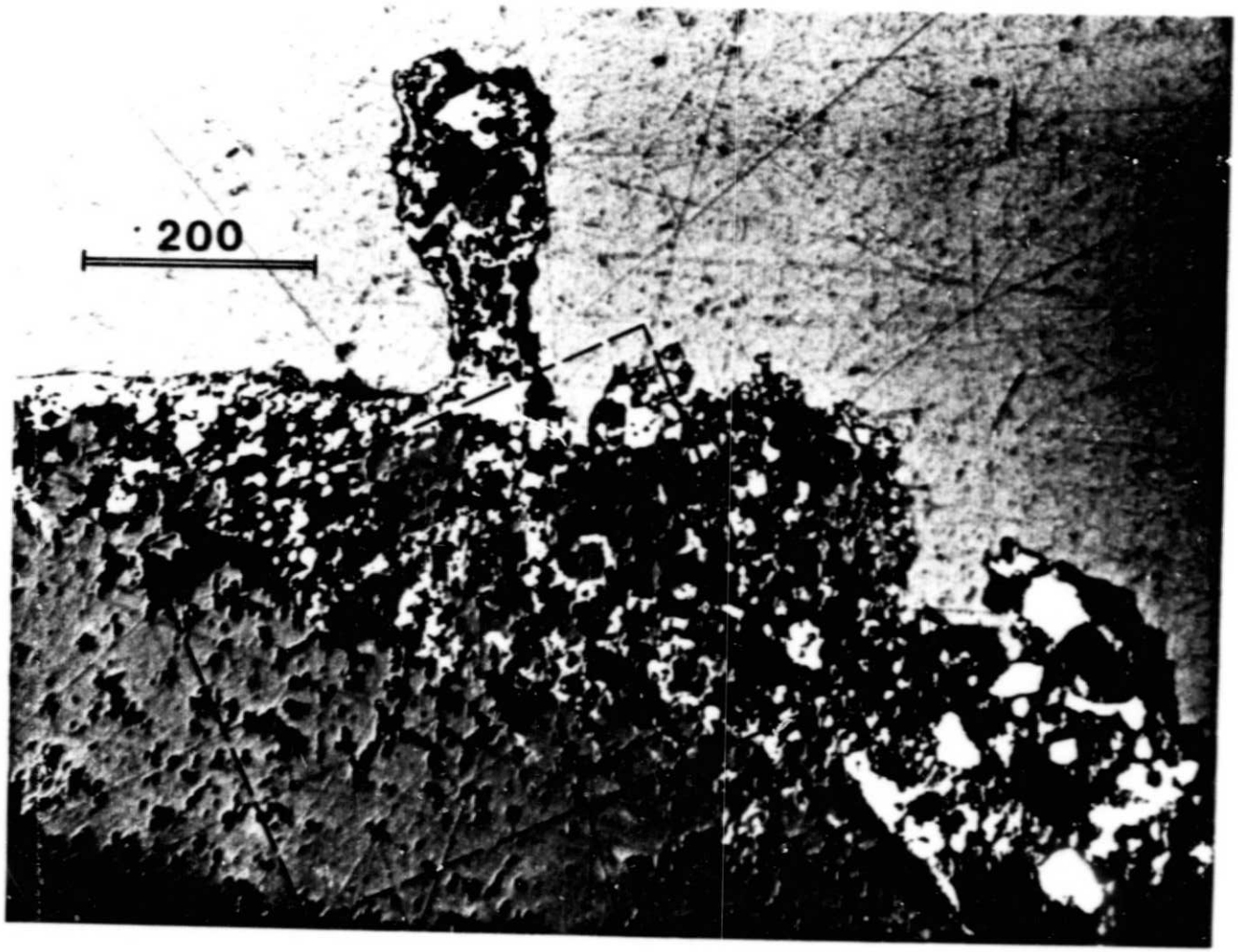

Fig. 6

TJA84201SFD

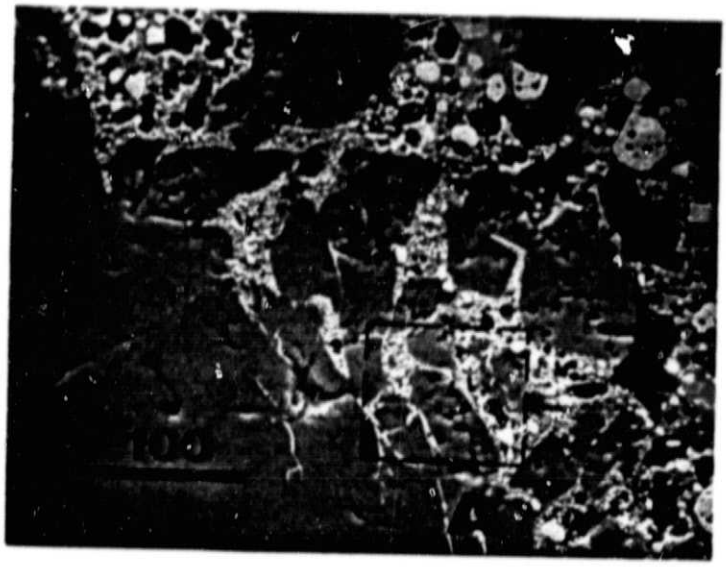

a)

b)

Fig. 7

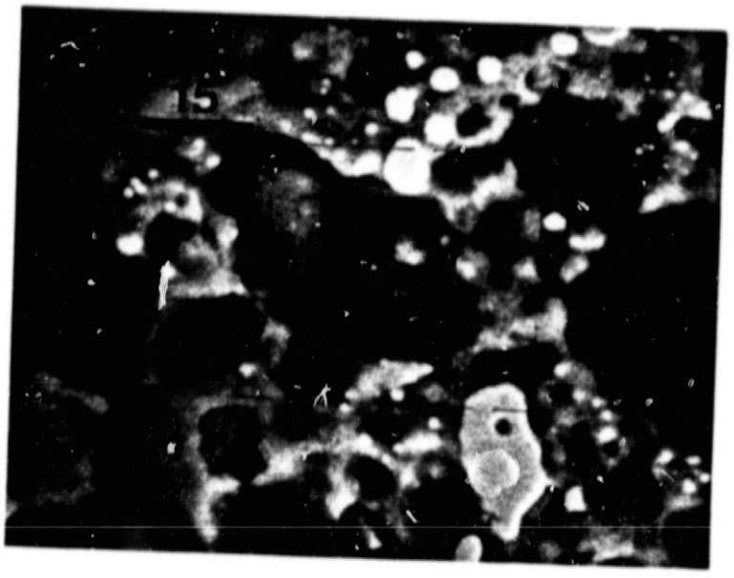

a)

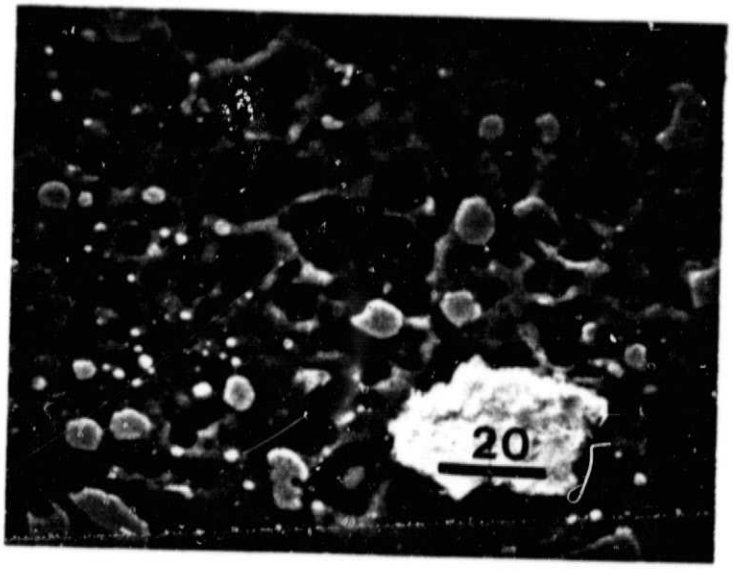

b)

Fig. 8

TJA84203SFD

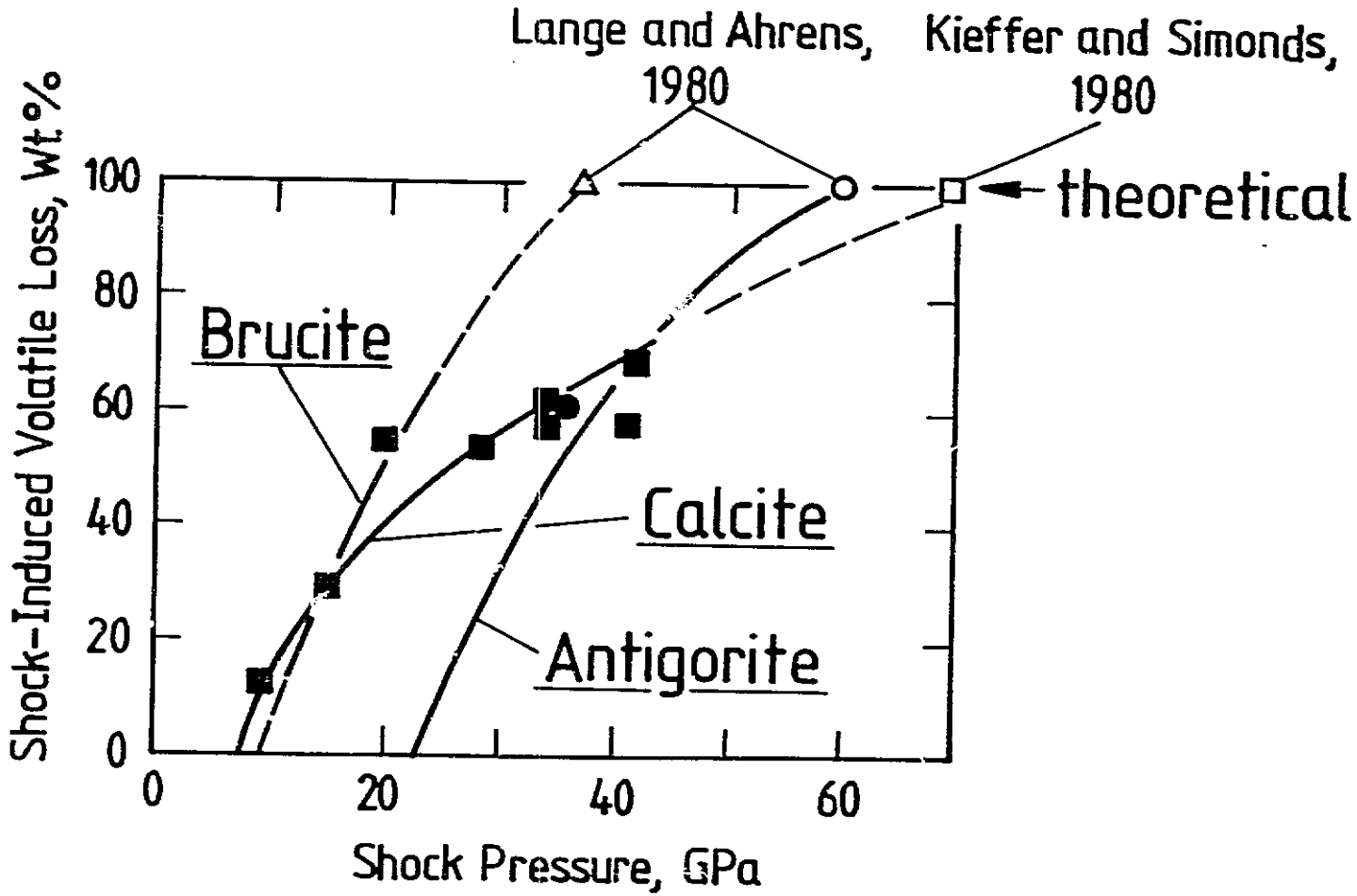

Fig. 9

TJA64204SFD

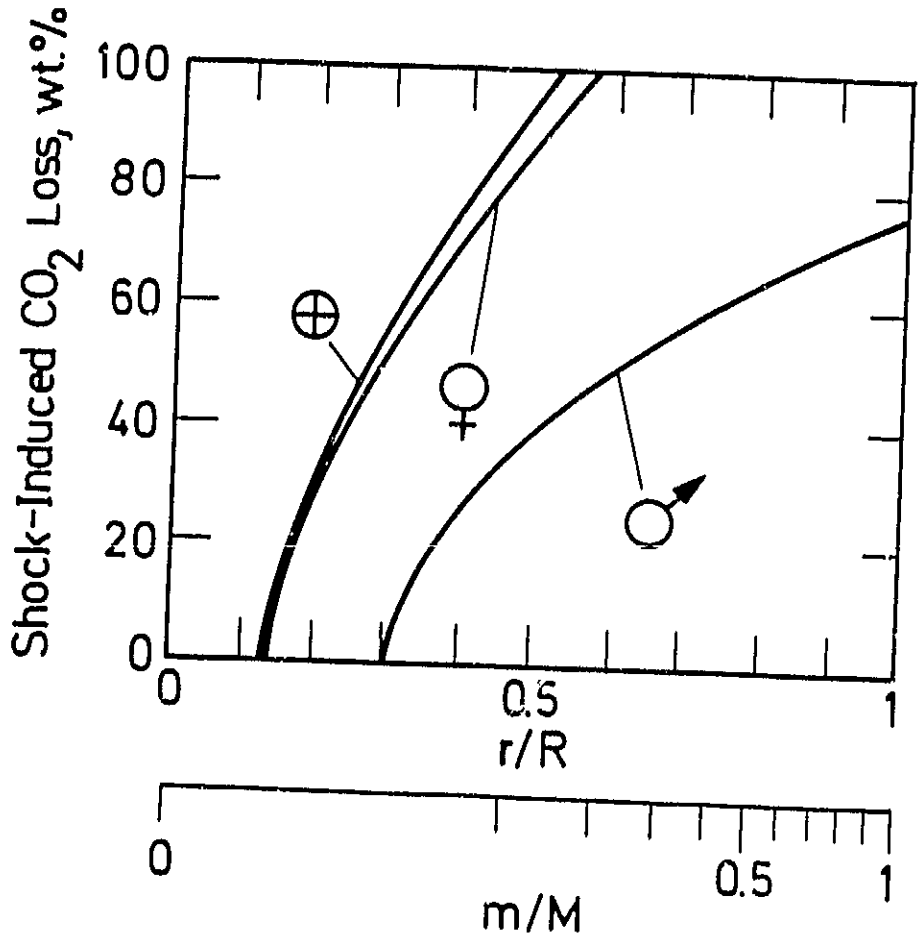

Fig. 10

TJA84205SFD